

The application of topological quantum chemistry in electrifieds

Simin Nie,^{1,2,*} Yuting Qian,^{1,3,*} Jiacheng Gao,^{1,3} Zhong Fang,^{1,3} Hongming Weng,^{1,3,4,†} and Zhijun Wang^{1,3,‡}

¹Beijing National Laboratory for Condensed Matter Physics,
and Institute of Physics, Chinese Academy of Sciences, Beijing 100190, China

²Department of Materials Science and Engineering,
Stanford University, Stanford, California 94305, USA

³University of Chinese Academy of Sciences, Beijing 100049, China

⁴Songshan Lake Materials Laboratory, Dongguan, Guangdong 523808, China

The recently developed theory of topological quantum chemistry (TQC) has built a close connection between band representations in momentum space and orbital characters in real space. It provides an effective way to diagnose topological materials, leading to the discovery of lots of topological materials after the screening of all known nonmagnetic compounds. On the other hand, it can also efficiently reveal spacial orbital characters, including average charge centers and site-symmetry characters. By using TQC theory, we demonstrate that the electrifieds with excess electrons serving as anions at vacancies can be well identified by analyzing band representations (BRs), which *cannot* be expressed as a sum of *atomic-orbital-induced* band representations (aBRs). By computing the irreducible representations of electronic states, we find that the floating bands (formed by the excess electrons) belong to the BRs induced from the “pseudo-orbitals” centered at vacancies, which can be characterized by real-space invariants (RSI), providing a promising avenue to pursue more electrifieds in ionic crystals.

I. INTRODUCTION

Recently, the discovery of topological materials has sprung up, and numerous nonmagnetic materials are predicted to be topologically nontrivial by first-principles calculations based on symmetry-based strategies [1–7], such as symmetry indicators [5, 6] and topological quantum chemistry (TQC) [7]. To be specific, the TQC theory first builds up the character tables for all k -points, and compatible relations (CR) for all 230 space groups (released on Bilbao Crystalline Server [8]), which make it possible to obtain the corresponding irreducible representations (irreps) of electronic states from first-principles calculations (*i.e.*, `irvsp` [9]). Then, it constructs a complete list of elementary band representations (eBRs), serving as its basic building blocks, which make a close link between the irreps in momentum space and the orbital characters in real space. In TQC theory, the trivial [*resp.* topological (crystalline)] insulators satisfy CR and can [*resp.* cannot] be expressed as a sum of eBRs, while the enforced topological semimetals violate the CR. Here, we emphasize that the TQC theory not only can diagnose topology of energy bands in momentum space, but also can reveal orbital characters in real space (*i.e.*, the average charge centers and site-symmetry characters) for a set of isolated bands. It is also noted that for topologically trivial insulators, we can further define the *unconventional* ones, whose BR decomposition has to contain an essential BR induced from a “pseudo-orbital” centered at a vacancy, which can be characterized by RSI [10]. In other words, the occupied bands of the *unconventional*

trivial insulators (also known as obstructed atomic limits) cannot be decomposed as a sum of aBRs (defined as the BR induced by the real atomic orbitals in crystals). To diagnose *unconventional* (trivial) states by TQC can be widely used in materials science [11], such as hydride storage materials [11], higher-order topological insulators (HOTIs) [12, 13], and electrifieds [14].

We here focus the TQC application in the electrifieds (check more applications in Ref. [11]). Electrifieds are defined as ionic crystals with excess electrons confined in particular cavities [15–18], whose arrangement determines the properties of electrifieds and gives their classification by the dimensionality [19–22]. The anionic electrons, being not attached to any atom, bond or molecule, exhibit high electron mobility and low work function, which have been experimentally confirmed in Ca_2N [18]: a two dimensional (2D) electrified with an excess electron per unit cell ($[\text{Ca}_2\text{N}]^+ \cdot e^-$). The low work function of electrified is beneficial to induce band inversion, and to realize the nontrivial band topology [14]. Recently, the concept of electrifieds with nontrivial band topology has attracted much attention for promising applications in quantum devices [14, 23–27]. Given the close relation between BRs and orbital characters, TQC may shed light on the origin of electrifieds in ionic materials.

Although there are many studies on searching for inorganic electrifieds, most of them are limited to compute charge distributions [19–22]. The symmetry analysis of electrifieds is lacking. In this paper, the BR analysis in the TQC provides a way to identify the origin of the bands around E_F from their symmetry eigenvalues (or irreps) alone, which can be used to find new electrified candidates effectively. We first introduce the concept of aBRs, which denote the BRs induced by real atomic orbitals in crystals and can be generated by our homemade code `pos2aBR`. Then we demonstrate that the electrifieds are the ionic

* These authors contributed equally to this work.

† hmweng@iphy.ac.cn

‡ wzj@iphy.ac.cn

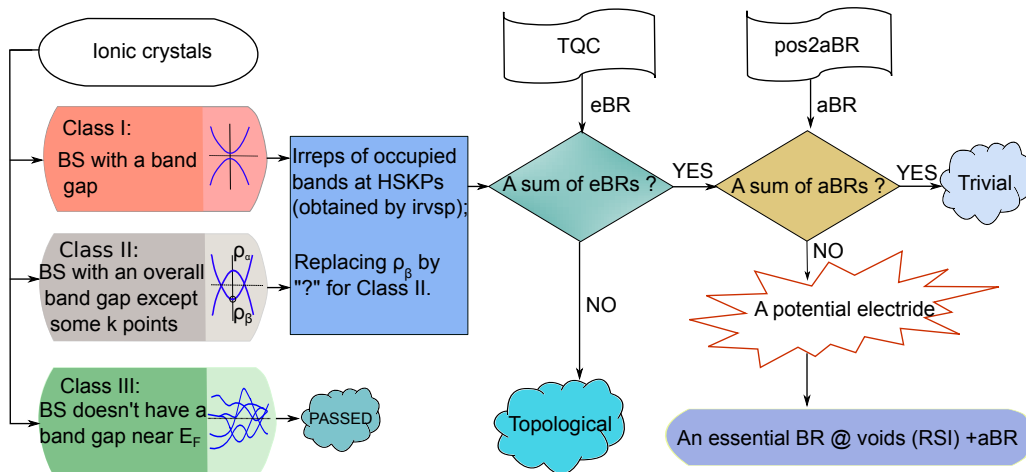


FIG. 1. (Color online). The workflow to find an electride candidate based on TQC. For a given ionic crystal, we first calculate the BS and classify it into three classes according to the (overall) band gap near E_F . In Class I, it has a direct band gap around E_F . In Class II, there is an overall band gap except some k-points. Apart from the two classes, those of Class III have many messy bands that can not be separated by a band gap. Then, we use the program `irvsp` to obtain the irreps of the occupied bands (below the band gap) at several high symmetry k-points (HSKPs). For Class II, we allow the irrep of the highest VB at the K point to be an arbitrary irrep by simply replacing “ ρ_β ” by the question mark “?”. The question mark can be assigned to any irrep when solving the BR decomposition. If the set of irreps for those bands is a sum of eBRs, but not a sum of aBRs, the ionic crystal can be considered as an electride candidate. Finally, we can decompose these bands into a sum of aBRs and an essential BR, which is characterized by the nonzero RSI at voids. The essential BR will specify the average charge centers and orbital characters of the excess electrons.

crystals, whose occupied bands are decomposed as a sum of eBRs, but not a sum of aBRs. At last, some potential electrides are predicted in ionic crystals by applying this criterion, which can be further checked in future experiments. The workflow of our method is given in Fig. 1, which works for both Class I with a clear band gap and Class II with the band inversion at a k-point. The materials with messy bands crossing E_F (Class III) are not considered further.

II. RESULTS AND DISCUSSION

To achieve an electride, it is empirically known that three criteria should be satisfied: excess electrons, lattice vacancies and suitable electronegativity of the elements. The previous search [19–22] for electrides have been done mainly by analyzing the charge density around the Fermi level (E_F), where electron localization function (ELF) analysis has proved to be effective. Here, by following the workflow (Fig. 1) within the TQC theory, we perform the analysis of irreps and BRs for electrides in first-principles calculations, leading to the well understanding of three characteristics of electrides. First, the floating bands are induced from the BRs of vacancies, indicating that their average charge densities are located at the vacancies in real space. Second, due to the loose confinement, the floating bands are usually close to the E_F , which is beneficial to induce band inversion and nontriv-

ial band topology. Third, the excess anionic electrons in cavities present a strong hydrogen affinity. The absorption of hydrogen usually moves those floating bands far below E_F and lowers the total energy.

A. Band representation of the pseudo-orbitals at voids

We take the compound Ca_2As as an example of Class I in Fig. 1, which has a body-centered tetragonal structure and space group $I4/mmm$ (SG #139). The lattice parameters are $a = 4.63 \text{ \AA}$, $c = 15.56 \text{ \AA}$. The As and Ca(1) occupy the Wyckoff sites (WKS) $4e$ $(0, 0, z)$ with $z = 0.135$ and 0.328 , respectively, while Ca(2) is at the $4c$ $(0, \frac{1}{2}, 0)$, as shown in Fig. 2 and Table I. It is worth noting that the $2b$ $(0, 0, \frac{1}{2})$ positions denoted by blue-dashed circles are hollow. In the (001) planes, the Ca and As atoms form 2D square lattices of Ca and As, respectively, which are stacked alternately along the z -direction, as shown in Fig. 2(a).

The band structure (BS) of Ca_2As with modified Becke-Johnson (mBJ) functional is shown in Fig. 2(b), where the size of the red and blue circles represents the weights of Ca- d and As- p orbitals, respectively. In addition to the presence of a global band gap in the BS, one can also find that the valence bands (VBs) are dominated by As- p orbitals, while the conduction bands (CBs) are mainly from Ca- d orbitals. Interestingly, since there are

TABLE I. Atomic positions and aBRs of Ca_2As (obtained by `pos2aBR`).

Atom	WKS(q)	Site symm.	Conf.	Irreps(ρ)	aBRs($\rho@q$)
As	4e	4mm	$4p^3$	p_z : A_1	$A_1@4e$
				p_x, p_y : E	$E@4e$
Ca(1)	4e	4mm	$4s^2$	s : A_1	$A_1@4e$
Ca(2)	4c	mmm	$4s^2$	s : A_g	$A_g@4c$

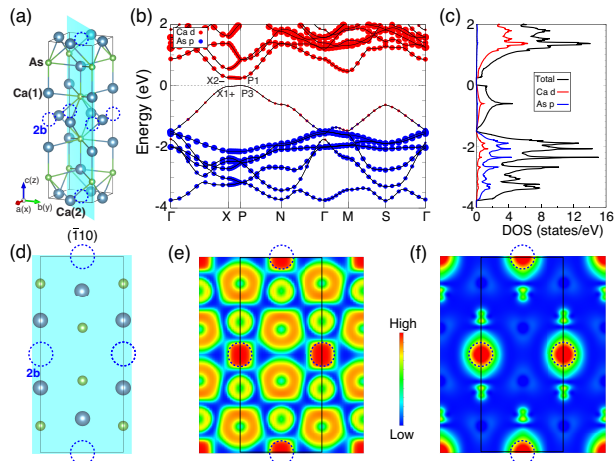


FIG. 2. (Color online) (a) Crystal structure and (d) $(\bar{1}10)$ lattice plane of Ca_2As . (b) The mBJ BS of Ca_2As with spectral weights of Ca- d and As- p orbitals represented by the size of the red and blue circles, respectively. (c) The orbital-resolved DOS of Ca_2As . (e) ELF of the total electron density of Ca_2As , and (f) PED for the states in the energy range -1.3 eV to 0 eV on the $(\bar{1}10)$ plane of Ca_2As . Hereafter, the corresponding cavity sites (*i.e.*, WKS $2b$ for Ca_2As) are depicted by blue-dashed circle.

7 VBs but only 6 As- p orbitals in a primitive cell, one can notice that the highest VB in the energy range -1.5 eV to 0 eV is not attributed to either As- p or Ca- d orbitals, which are consistent with the orbital-resolved density of states (DOS), as shown in Fig. 2(c). In what follows, we will show that the band does not belong to any aBR.

To check the orbital characters of the 7 well-isolated VBs in the energy range -4 eV to 0 eV, we have done the analysis of irreps and BRs for these VBs, which are presented in Table II. We find that these VBs can be decomposed into a sum of BRs: $(A_1 + E)@4e \oplus A_{1g}@2b$. Here, a BR of $\rho@q$ is formed by the states of ρ irrep centered at the WKS q . In view of all the aBRs of this compound obtained by `pos2aBR` given in Table I, the BR analysis indicates that the lowest six bands [*i.e.*, $(A_1 + E)@4e$] are consistent with the states formed by the p_x, p_y, p_z orbitals of As (*i.e.*, WKS 4e), which agrees well with the fatted BS [Fig. 2(b)]. Interestingly, the remaining band (*i.e.*, $A_{1g}@2b$) is contributed from a specific eBR generated by a free electron e^- located at the cavity $2b$. Therefore, the BR decomposition of Ca_2As is not a sum of aBRs, indicating that Ca_2As is an electride candidate in terms of symme-

TABLE II. Irreps (obtained by `irvsp`) and BRs (copied from TQC) for the 7 VBs of Ca_2As . The BR colored in blue is generated by an excess electron e^- located at vacancies. Hereafter, the irreps are given in the order of increasing energy eigenvalues, and the number in the bracket denotes the degeneracy of the irrep.

	Γ (GM)	M	P	X	N
Bands	GM1+(1)	M1+(1)	P5(2)	X4-(1)	N2-(1)
	GM5+(2)	M3-(1)	P5(2)	X3-(1)	N1+(1)
	GM1+(1)	M5+(2)	P1(1)	X4+(1)	N1+(1)
	GM3-(1)	M5-(2)	P3(1)	X1+(1)	N2+(1)
	GM5-(2)	M1+(1)	P3(1)	X3+(1)	N2-(1)
				X2-(1)	N1-(1)
			X1+(1)	N2-(1)	
BRs					
$A_1@4e$	GM3-(1)	M3-(1)	P3(1)	X2-(1)	N2-(1)
	GM1+(1)	M1+(1)	P1(1)	X1+(1)	N1+(1)
$E@4e$	GM5-(2)	M5-(2)	P5(2)	X3-(1)	N1-(1)
	GM5+(2)	M5+(2)	P5(2)	X3+(1)	N1+(1)
				X4-(1)	N2-(1)
				X4+(1)	N2+(1)
$A_{1g}@2b$	GM1+(1)	M1+(1)	P3(1)	X1+(1)	N2-(1)

tries and irreps. In addition, the RSI for the $2b$ WKS (with time reversal) for SG #139 can be computed to be $\delta_1 [\equiv -m(A_{1g}) + m(A_{2g}) - m(A_{1u}) + m(A_{2u})] = -1$ [11] [$m(\rho)$ denotes the number of the irrep ρ]. The nonzero $\delta_1@2b$ indicates the essentiality of the BR from $2b$.

In addition to the analysis of BRs in TQC, the charge density distribution can be clearly visualized. In Figs. 2(e) and 2(f), we plot the ELF of all valence states and partial electron density (PED) of the states in the energy range -1.3 eV to 0 eV on $(\bar{1}10)$ plane for Ca_2As , respectively, which both suggest the existence of excess electron distribution at the vacancies (*i.e.*, the WKS $2b$) and the chemical view of the stoichiometric electride $(\text{Ca}_2\text{As})^+ \cdot e^-$. Once the surface termination cuts through the vacancies (*i.e.*, the charge centers of the floating bands), floating surface states are expected [14, 28]. The similar analysis can be also applied to other well-known electrides of Class I: Ca_2N [18], LaCl [20], and $\text{Ca}_{24}\text{Al}_{28}\text{O}_{64}$ (called C12A7 for short) [17], which can be found in Sections B and C of the Supplementary Material.

B. Band inversion at the Fermi level

It is well-known that topological materials always have a band inversion near E_F . Compared with the states constrained by nuclei, the floating states are more conductive, and usually very close to the E_F . Given the very likely presence of the band inversion between the floating bands and other energy bands around E_F , it is natural to expect nontrivial band topology in electrides, resulting in the discovery of various topological states in electrides. Next, the BR analysis will show that the band inversion

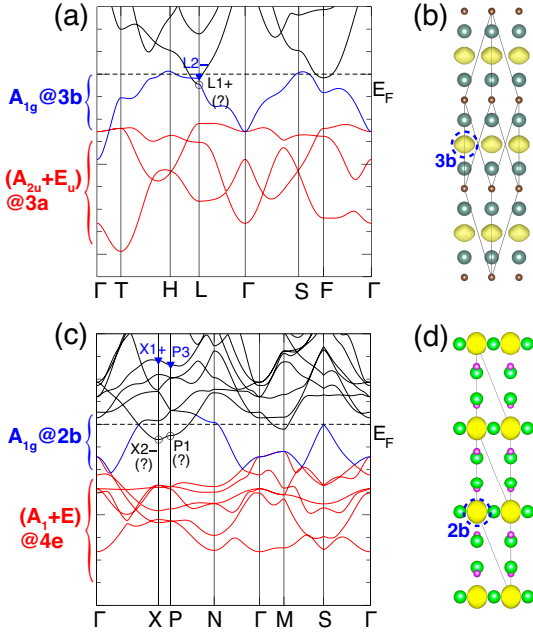


FIG. 3. (Color online) (a) BSs of Y_2C with GGA. (c) BSs of Ba_2Bi with mBJ modification. The irreps $L1+$, $X2-$, $P1$ replaced by “?” can be respectively assigned to the irrep $L2-$, $X1+$, $P3$ marked by blue filled triangles after solving the BR decomposition. The braces show the BRs produced by the bands in the corresponding energy ranges. The PED of the highest VBs for Y_2C (b) and Ba_2Bi (d).

in electride usually comes from eBRs of the interstitial positions.

Here we take Y_2C with as an example of Class II for illustrating the application of TQC in topological electrides. It crystallizes in an anti- $CdCl_2$ type structure with the SG of $R\bar{3}m$ (SG #166). In the generalized gradient approximation (GGA) calculation [29] [Fig. 3(a)], a band inversion is clearly denoted by the irreps ($L2-$ and “?”) of the two low-energy bands at L, which contributes to a nodal-line structure traversing the full Brillouin zone (BZ) without spin-orbit coupling (SOC) [14]. The aBRs and the analysis of irreps for Y_2C are shown in Table III and Table IV, respectively. After replacing the highest VB irrep “ $L1+$ ” by “?”, the only solution of BR decomposition for the VBs in Y_2C is $(A_{2u} + E_u)@3a \oplus A_{1g}@3b$. The aBRs $(A_{2u} + E_u)@3a$ originate from C- p orbitals, while the eBR $A_{1g}@3b$ is formed by an excess electron at the vacancy site $3b$. The “?” is solved to be “ $L2-$ ” instead of “ $L1+$ ”, suggesting that the Y_2C is an electride with a band inversion. The essential eBR of the “floating” band is characterized by the computed $\delta_1@3b \equiv -m(A_{1g}) - m(A_{2g}) + m(A_{1u}) + m(A_{2u}) = -1$ for SG #166 [11]. The PED of the states colored in blue is also explored to confirm its electride feature, as shown in Fig. 3(b). The presence of charge distribution at the vacancies (*i.e.*, WKS $3b$) is consistent with the BR and RSI analysis.

The electrides A_2B ($A = Ca, Sr, \text{ and } Ba; B = As,$

TABLE III. Atomic positions and aBRs of Y_2C (obtained by `pos2aBR`).

Atom	WKS(q)	Site symm.	Conf.	Irreps(ρ)	aBRs($\rho@q$)
Y	6c	3m	$5s^25d^2$	$s, d : \rho$	$\rho@6c$
C	3a	$-3m$	$2p^2$	$p_z : A_{2u}$ $p_x, p_y : E_u$	$A_{2u}@3a$ $E_u@3a$

TABLE IV. Irreps (obtained by `irvsp`) and BRs (copied from TQC) for the four VBs near the Fermi level of Y_2C . The question mark (“?”) stands for any 1D irrep (*i.e.*, the unknown irrep) at L. After analyzing the BRs of the occupied bands, one then can conjecture that the unknown irrep should be $L2-(1)$.

	Γ	T	F	L
Bands	GM2-(1)	T2-(1)	F2-(1)	L2-(1)
	GM1+(1)	T3-(2)	F2-(1)	L2-(1)
	GM3-(2)	T2-(1)	F1-(1)	L1-(1)
			F1+(1)	? (1)
BRs				
$A_{2u}@3a$	GM2-(1)	T2-(1)	F2-(1)	L2-(1)
$E_u@3a$	GM3-(2)	T3-(2)	F1-(1) \oplus F2-(1)	L1-(1) \oplus L2-(1)
$A_{1g}@3b$	GM1+(1)	T2-(1)	F1+(1)	L2-(1)

Sb, and Bi) with the SG of $I4/mmm$ (SG #139) are also reported topological nodal-line materials without SOC [26, 30]. The mBJ BSs for these materials can be found in Section D of the Supplementary Material. As shown above, Ca_2As is a trivial electride with a global band gap in the BZ (*i.e.*, Class I). As the components vary from Ca/As to Ba/Bi, the band inversion occurs in Ba_2Bi (*i.e.*, Class II), as shown in Fig. 3(c), leading to the nodal line protected by the coexistence of space inversion and time-reversal symmetries. After replacing the highest VB irreps $X2-$ and $P1$ of Ba_2Bi by “?”, similar to Ca_2As , we can obtain the highest VB from the eBR $A_{1g}@2b$ by solving BR decomposition. Although the floating band of $A_{1g}@2b$ is not fully occupied and has a band inversion with the lowest CB, Ba_2Bi can still be considered as an electride with nontrivial band topology. As expected, the PED of Ba_2Bi shows the charge densities at the cavity $2b$ in Fig. 3(d). In fact, the Ca_2As family have lots of compounds, which are all electride candidates (See Section D of the Supplementary Material).

C. Hydrogen absorption

The electrides, with excess electrons serving as anions at vacancies, are very easy to absorb hydrogen atoms at the vacancies, which would move the floating bands far away from E_F . In order to understand the absorption process, we show the results of Ca_5P_3 and Ba_3CrN_3 as two paradigms. Ca_5P_3 crystallizes in a Mn_5Si_3 -type structure with the SG of $P6_3/mcm$ (SG #193), and its electronic structure is shown in Fig. 4(a). The BR anal-

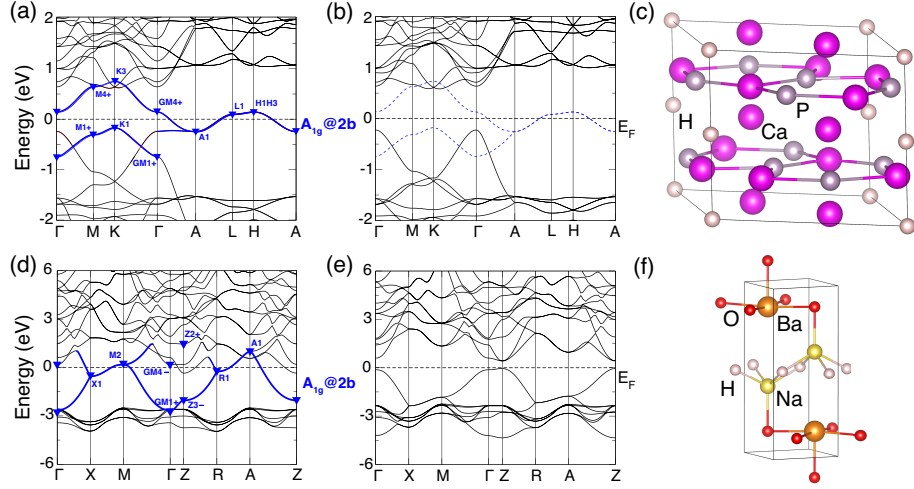


FIG. 4. (Color online) The BSs of Ca_5P_3 (a), $\text{Ca}_5\text{P}_3\text{H}$ (b), NaBaO (d) and NaBaOH (e). The floating bands (blue-solid) in Ca_5P_3 , and NaBaO denote electronic states of excess electrons, whose eBRs can be well determined by the obtained irreps. To facilitate the comparison, the irreps of particular bands are marked out, and the “disappeared” floating bands for $\text{Ca}_5\text{P}_3\text{H}$ are depicted by blue-dashed lines in (b). (c,f) The crystal structures of $\text{Ca}_5\text{P}_3\text{H}$ and NaBaOH , respectively.

ysis shows that these blue-solid bands of Ca_5P_3 are the states formed by excess electrons at vacancies, since the eBR $A_{1g}@2b$ is determined by the obtained irreps labeled in Fig. 4(a). After absorption of hydrogen atoms at $2b$ as shown in Fig. 4(c), the floating bands move far below E_F in $\text{Ca}_5\text{P}_3\text{H}$ [Fig. 4(b)], because the hydrogen atoms will bond with the surrounding electrons producing a strong interaction, which is consistent with previous work [31]. The similar analysis of Ba_3CrN_3 can be found in Section E of the Supplementary Material. Therefore, the process of adsorbing hydrogen atoms confirms the results of the BR analysis, and strongly supports the presence of the excess electrons at cavities in electrides.

D. Prediction of electride candidates

Based on the above discussions on three aspects, we find that the TQC theory is very implementable in the understanding of various properties of electrides. Guided by this finding, we predict some potential electrides in ionic crystals by following the workflow in Fig. 1. We first propose that NaBaO [32] with the SG of $P4/nmm$ (SG #129) could be an electride with an excess electron located at the cavity $2b$, since the BR of the floating bands [denoted by blue-colored lines and irreps in Fig. 4(d)] is elementary, and the average charge center is located at the cavity. In fact, these floating bands are half-filled. By absorbing a hydrogen atom at $2b$ [as shown in Fig. 4(f)], the floating bands move completely below E_F , as shown in Fig. 4(e).

Next we also find that Sr_6GaN_5 could be an electride after electron doping, *i.e.*, $\text{Sr}_6\text{Ga}_{0.5}\text{Ge}_{0.5}\text{N}_5$ which is similar to the case of $\text{K}_2\text{O}_{0.5}\text{F}_{0.5}$ by doping K_2O [19]. The BS of K_2O with the SG of $Fm\bar{3}m$ (SG #225) is

shown in Fig. 5(a). Above E_F , we can see there is an isolated band (blue-colored) in the energy range 1 eV to 4 eV. With the obtained irreps at HSKPs, the BR analysis shows that this band belongs to the eBR of $A_{1g}@4b$, which suggests that the band is formed by an excess electron at cavity $4b$. By doping 50% O with F, the isolated band is partially occupied in $\text{K}_2\text{O}_{0.5}\text{F}_{0.5}$. The presence of a spherical charge distribution around the cavity in the PED of this band [Fig. 5(b)] also confirms that $\text{K}_2\text{O}_{0.5}\text{F}_{0.5}$ is an electride. Heuristically, we propose that Sr_6GaN_5 with a hexagonal structure of $P6_3/mcm$ (SG #193) could also be an electride after electron doping.

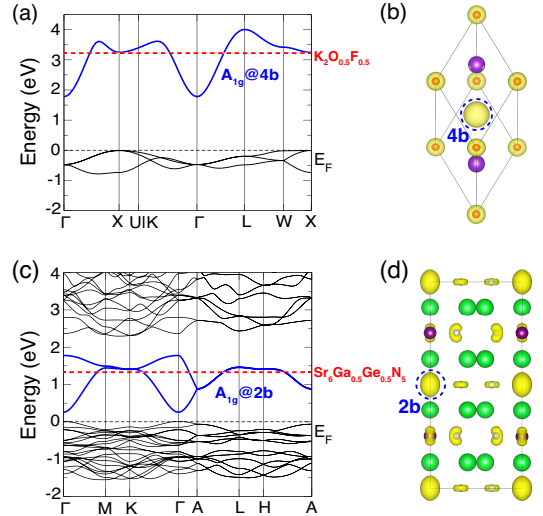


FIG. 5. (Color online) The calculated BSs and PED of the floating bands (blue-colored) for K_2O (a,b) and Sr_6GaN_5 (c,d). The Fermi levels of $\text{K}_2\text{O}_{0.5}\text{F}_{0.5}$ and $\text{Sr}_6\text{Ga}_{0.5}\text{Ge}_{0.5}\text{N}_5$ are indicated by red-dashed lines.

Its BS is shown in Fig. 5(c). We find two well-isolated CBs (blue-colored) form the eBR of $A_{1g}@2b$, indicating the corresponding charge centers at $2b$, which are consistent with the calculated PED [Fig. 5(d)]. By electron doping, the floating bands of Sr_6GaN_5 are half-filled in $\text{Sr}_6\text{Ga}_{0.5}\text{Ge}_{0.5}\text{N}_5$, as shown in Fig. 5(c). More details of these two predicted materials, and the results of another candidate (Sr_3P_2) can be found in Section F of the Supplementary Material.

E. Discussion

Through the BR analysis in the TQC with the obtained irreps at HSKPs, one can effectively identify the average electronic charge centers and the corresponding site-symmetry characters for a set of separated bands, providing an ideal avenue to both understand the essence of the well-known electrifieds and find new candidates in the future. Our methodology will facilitate the study of the interesting properties of electrifieds, such as high electron mobility and low work function. More interestingly, more fundamental physical phenomena can be found in the electrifieds after considering interactions, such as Sr_5P_3 and Zr_5Sb_3 .

Sr_5P_3 has two different structures with the SG of $C2/m$ (SG #12; quasi-hexagonal form) and the SG of $P6_3/mcm$ (SG #193; hexagonal form) at ambient and high pressures, respectively. The atoms in the quasi-hexagonal form deviate somewhat from that of the hexagonal form, and the hexagonal Sr_5P_3 shares the same crystal structure and similar BS of Ca_5P_3 . Thus, they are all expected to be electrifieds with half-filled floating bands. However, the obtained metallic BS in the GGA calculation is in contrast with the observed insulator-type conductivity in experiments [22]. To remedy this discrepancy, the spin-polarized calculation and Coulomb-U effect have been considered in Ref. [18] and a tiny band gap can be found, resulting in the formation of lower and upper Hubbard bands with DOS peaks below and above E_F , respectively. They conjecture that this electrified may be a Mott insulator due to the effect of the on-site Coulomb interaction. In addition, the phase transition from the hexagonal form (high pressure) to the quasi-hexagonal form (ambient pressure) also suggests the possible presence of a charge-density-wave transition.

Zr_5Sb_3 is experimentally found to be the first superconductor in the large family of compounds with Mn_5Si_3 -type structure (SG #193) [33], which are believed to be due to the electron-phonon coupling. Although the GGA BS is a little complicated, after carefully checking the irreps of the occupied bands, we find that their irreps could be decomposed into a sum of BRs: $(A+B_1+B_2)@6g$ (Sb atoms), $(A_1+E)@4d$ [Zr(2) atoms] and $A_1'@2a$ (which is hollow). By electron counting, the floating bands of eBR $A_1'@2a$ are 1/4 filled, and create large Fermi surfaces. When the interstitial sites are filled by extra Sb atoms, the experimental measurements have also found that the

superconductivity in $\text{Zr}_5\text{Sb}_{3+x}$ is suppressed. Similar results are also obtained in $\text{Zr}_5\text{Sb}_3\text{O}$ and $\text{Zr}_5\text{Sb}_3\text{C}$. These experiments suggest that the superconductivity may be related to the anionic excess electrons at the interstitial sites.

III. CONCLUSIONS

In conclusion, we demonstrate that the analysis of irreps and BRs in the TQC theory provides an effective way to identify the origin of the bands around E_F from their symmetry eigenvalues (or irreps) alone, which is extremely useful to find new electrified candidates. The electrifieds can be considered as the trivial ionic crystals with nonzero RSI at vacancies. A brief workflow is given as well for the search of electrifieds. In addition, three characteristics of electrifieds can be well understood in the TQC theory. First, since there are floating bands with charge densities centered at vacancies in real space, surface states could emerge when the surface termination cuts through these vacancies. Second, as the excess electrons show the lack of strong confinement, low work function and floating bands close to E_F are expected. Consequently, the band inversion and nontrivial band topology are very like to happen in electrified. Third, the interstitial anionic electrons are easy to absorb hydrogen atoms, which would move the floating bands far away from E_F and gain the benefit in total energy. More generally, in the TQC theory, the hydrogen storage materials and 2D HOTIs can be known as metal alloys and covalent compounds with trivial occupied bands being not a sum of aBRs, respectively. Anyway, the disagreement between the average charge centers and the atomic positions can be well described by the TQC theory, which can be widely used in the *unconventional* materials, such as electrifieds, hydrogen storage materials and HOTIs [11].

Theoretical methods — The Vienna *ab initio* simulation package (VASP) [34, 35] with the projector augmented wave method [36, 37] based on density functional theory was employed for the first-principles calculations. The GGA of Perdew-Burke-Ernzerhof type [29] was used for exchange-correlation potential. The cut-off energy for plane wave expansion was set to 500 eV. A $7 \times 7 \times 7$ Monkhorst-Pack grid for BZ sampling was supplied in the self-consistent process. A width of 0.02 eV was adopted in the Gaussian smearing method for Fermi level determination. All the BSs were calculated without considering SOC. In order to get more reliable BSs for the Ca_2As family, more accurate calculations with mBJ potential [38] were performed. The virtual crystal approximation [39] was employed to study the electronic structures of $\text{K}_2\text{O}_{0.5}\text{F}_{0.5}$ and $\text{Sr}_6\text{Ga}_{0.5}\text{Ge}_{0.5}\text{N}_5$.

The code pos2aBR — The code `pos2aBR` is developed to get the aBRs from a given crystal structure (*i.e.*, POSCAR) for 230 SGs. It converts “POSCAR” to “POSCAR_std”, which is compatible with the program `irvsp` and TQC work [7, 40–42]. Its standard output

contains the WKS (q) for each atom and the irreps (ρ) for

atomic orbitals (*i.e.*, s , p , d orbitals) in “POSCAR_std”. An example of the output for Y_2C is shown below

```

166 R-3m
\\
SN  Mult.  Wyck.  Atom  s    p    d  Wyck.  Name
   1     2     7    39    3    6    2   6c    Y
   2     1     9     6    2    2    0   3a    C
\\
SN  Orb. @ Site      Symm.      BCS  CJB  MUL
   1  Y-s @ 6c( 7)   3m(19) >>>  (1) (2) (3)      Basis
                        1  GM1 ;GM1 ; A1 ;      z ;x2+y2 ;z2
   1  Y-p @ 6c( 7)   3m(19) >>>  (1) (2) (3)      Basis
                        1  GM1 ;GM1 ; A1 ;      z ;x2+y2 ;z2
                        3  GM3 ;GM3 ; E  ;      x ,y ;xz ,yz ;x2-y2 ,xy ;Jx ,Jy
   1  Y-d @ 6c( 7)   3m(19) >>>  (1) (2) (3)      Basis
                        1  GM1 ;GM1 ; A1 ;      z ;x2+y2 ;z2
                        3  GM3 ;GM3 ; E  ;      x ,y ;xz ,yz ;x2-y2 ,xy ;Jx ,Jy
                        3  GM3 ;GM3 ; E  ;      x ,y ;xz ,yz ;x2-y2 ,xy ;Jx ,Jy
   2  C-s @ 3a( 9)   -3m(20) >>>  (1) (2) (3)      Basis
                        1  GM1+ ;GM1+ ; A1g ;      x2+y2 ;z2
   2  C-p @ 3a( 9)   -3m(20) >>>  (1) (2) (3)      Basis
                        4  GM2- ;GM2- ; A2u ;      z
                        6  GM3- ;GM3- ; Eu  ;      x ,y

```

Acknowledgments — This work was supported by the National Natural Science Foundation of China (Grants No. 11974395, No. 11504117), the Strategic Priority Research Program of Chinese Academy of Sciences (Grant No. XDB33000000), and the Center for Materials Genome. H.W. acknowledges support from the Ministry of Science and Technology of China under

grant numbers 2016YFA0300600 and 2018YFA0305700, the Chinese Academy of Sciences under grant number XDB28000000, the Science Challenge Project (No. TZ2016004), the K. C. Wong Education Foundation (GJTD-2018-01), Beijing Municipal Science & Technology Commission (Z181100004218001) and Beijing Natural Science Foundation (Z180008).

- [1] F. Tang, H. C. Po, A. Vishwanath, and X. Wan, *Nature* **566**, 486 (2019).
- [2] F. Tang, H. C. Po, A. Vishwanath, and X. Wan, *Nature Physics* **15**, 470 (2019).
- [3] T. Zhang, Y. Jiang, Z. Song, H. Huang, Y. He, Z. Fang, H. Weng, and C. Fang, *Nature* **566**, 475 (2019).
- [4] M. G. Vergniory, L. Elcoro, C. Felser, N. Regnault, B. A. Bernevig, and Z. Wang, *Nature* **566**, 480 (2019).
- [5] H. C. Po, A. Vishwanath, and H. Watanabe, *Nature communications* **8**, 1 (2017).
- [6] Z. Song, T. Zhang, Z. Fang, and C. Fang, *Nature communications* **9**, 1 (2018).
- [7] B. Bradlyn, L. Elcoro, J. Cano, M. Vergniory, Z. Wang, C. Felser, M. I. Aroyo, and B. A. Bernevig, *Nature* **547**, 298 (2017).
- [8] “Bilbao crystallographic server,” <https://www.cryst.ehu.es/cgi-bin/cryst/programs/bandrep.pl>.
- [9] J. Gao, Q. Wu, C. Persson, and Z. Wang, arXiv preprint arXiv:2002.04032 (2020).
- [10] Z.-D. Song, L. Elcoro, and B. A. Bernevig, *Science* **367**, 794 (2020), <https://science.sciencemag.org/content/367/6479/794.full.pdf>.
- [11] Qian, Yuting and others. Work in progress.
- [12] X.-L. Sheng, C. Chen, H. Liu, Z. Chen, Z.-M. Yu, Y. Zhao, and S. A. Yang, *Physical Review Letters* **123**, 256402 (2019).
- [13] E. Lee, R. Kim, J. Ahn, and B.-J. Yang, *npj Quantum Materials* **5**, 1 (2020).
- [14] M. Hirayama, S. Matsuishi, H. Hosono, and S. Murakami, *Physical Review X* **8**, 031067 (2018).
- [15] S. B. Dawes, D. L. Ward, R. H. Huang, and J. L. Dye, *Journal of the American Chemical Society* **108**, 3534 (1986).
- [16] J. L. Dye and M. G. DeBacker, *Annual Review of Physical Chemistry* **38**, 271 (1987).
- [17] S. Matsuishi, Y. Toda, M. Miyakawa, K. Hayashi, T. Kamiya, M. Hirano, I. Tanaka, and H. Hosono, *Science* **301**, 626 (2003).
- [18] K. Lee, S. W. Kim, Y. Toda, S. Matsuishi, and H. Hosono, *Nature* **494**, 336 (2013).
- [19] T. Tada, S. Takemoto, S. Matsuishi, and H. Hosono, *Inorganic chemistry* **53**, 10347 (2014).
- [20] Y. Zhang, H. Wang, Y. Wang, L. Zhang, and Y. Ma, *Physical Review X* **7**, 011017 (2017).
- [21] T. TADA, J. Wang, and H. Hosono, *Journal of Computer Chemistry, Japan* **16**, 135 (2017).
- [22] J. Wang, K. Hanzawa, H. Hiramatsu, J. Kim, N. Umezawa, K. Iwanaka, T. Tada, and H. Hosono,

- Journal of the American Chemical Society **139**, 15668 (2017).
- [23] H. Huang, K.-H. Jin, S. Zhang, and F. Liu, Nano letters **18**, 1972 (2018).
- [24] S. Nie, B. A. Bernevig, and Z. Wang, arXiv preprint arXiv:2006.12502 (2020).
- [25] S.-C. Zhu, L. Wang, J.-Y. Qu, J.-J. Wang, T. Frolov, X.-Q. Chen, and Q. Zhu, Physical Review Materials **3**, 024205 (2019).
- [26] X. Zhang, B. Fu, L. Jin, X. Dai, G. Liu, and Y. Yao, The Journal of Physical Chemistry C **123**, 25871 (2019).
- [27] S. Nie, H. Weng, and F. B. Prinz, Physical Review B **99**, 035125 (2019).
- [28] I. Tateishi, .
- [29] J. P. Perdew, K. Burke, and M. Ernzerhof, *Phys. Rev. Lett.* **77**, 3865 (1996).
- [30] X. Zhang, Z.-M. Yu, Y. Lu, X.-L. Sheng, H. Y. Yang, and S. A. Yang, Physical Review B **97**, 125143 (2018).
- [31] L. S. Xie, L. M. Schoop, E. M. Seibel, Q. D. Gibson, W. Xie, and R. J. Cava, Apl Materials **3**, 083602 (2015).
- [32] J. Deng, J. Guo, and X. Chen, Journal of the American Chemical Society **142**, 5234 (2020).
- [33] B. Lv, X. Y. Zhu, B. Lorenz, F. Y. Wei, Y. Y. Xue, Z. P. Yin, G. Kotliar, and C. W. Chu, *Phys. Rev. B* **88**, 134520 (2013).
- [34] G. Kresse and J. Furthmüller, *Phys. Rev. B* **54**, 11169 (1996).
- [35] G. Kresse and J. Furthmüller, *Computational Materials Science* **6**, 15 (1996).
- [36] P. E. Blöchl, *Phys. Rev. B* **50**, 17953 (1994).
- [37] G. Kresse and D. Joubert, *Phys. Rev. B* **59**, 1758 (1999).
- [38] F. Tran and P. Blaha, Physical review letters **102**, 226401 (2009).
- [39] L. Nordheim, *Ann. Phys* **9**, 607 (1931).
- [40] J. Cano, B. Bradlyn, Z. Wang, L. Elcoro, M. Vergniory, C. Felser, M. Aroyo, and B. A. Bernevig, Physical Review B **97**, 035139 (2018).
- [41] M. Vergniory, L. Elcoro, Z. Wang, J. Cano, C. Felser, M. Aroyo, B. A. Bernevig, and B. Bradlyn, Physical Review E **96**, 023310 (2017).
- [42] J. Cano, B. Bradlyn, Z. Wang, L. Elcoro, M. Vergniory, C. Felser, M. Aroyo, and B. A. Bernevig, Physical review letters **120**, 266401 (2018).
- [43] A. Togo and I. Tanaka, “Spglib: a software library for crystal symmetry search,” (2018), arXiv:1808.01590 [cond-mat.mtrl-sci].
- [44] B. Bradlyn, L. Elcoro, J. Cano, M. Vergniory, Z. Wang, C. Felser, M. Aroyo, and B. A. Bernevig, Nature **547**, 298 (2017).
- [45] M. I. Aroyo, J. Perez-Mato, D. Orobengoa, E. Tasci, G. de la Flor, and A. Kirov, Bulg. Chem. Commun **43**, 183 (2011).
- [46] M. I. Aroyo, J. M. Perez-Mato, C. Capillas, E. Kroumova, S. Ivantchev, G. Madariaga, A. Kirov, and H. Wondratschek, Zeitschrift für Kristallographie-Crystalline Materials **221**, 15 (2006).
- [47] M. I. Aroyo, A. Kirov, C. Capillas, J. Perez-Mato, and H. Wondratschek, Acta Crystallographica Section A: Foundations of Crystallography **62**, 115 (2006).
- [48] C. J. Bradley and A. P. Cracknell, “The mathematical theory of symmetry in solids.” (1972).
- [49] J. Wang, X. Sui, S. Gao, W. Duan, F. Liu, and B. Huang, *Phys. Rev. Lett.* **123**, 206402 (2019).
- [50] N. W. Falb, J. N. Neu, T. Besara, J. B. Whalen, D. J. Singh, and T. Siegrist, Inorganic chemistry **58**, 3302 (2019).

SUPPLEMENTARY INFORMATION

A. The code `pos2aBR`

The program `pos2aBR` is developed to get the aBRs from a given crystal structure (*i.e.*, POSCAR). The `Spglib` library [43] is needed for the program. After installing the `Spglib` library and copying `libsymspg.a` to the `src_pos2aBR` folder, the executable binary `pos2aBR` can be compiled by typing the following commands:

```
$ ./configure.sh
$ source ~/.bashrc
$ make
```

Before running `pos2aBR`, you would better standardize the POSCAR by using `phonopy`. A typical workflow of `pos2aBR` is shown as follows:

```
$ phonopy --symmetry --tolerance 0.01 -c POSCAR
$ cp PPOSCAR POSCAR
$ pos2aBR
```

The program `pos2aBR` converts “POSCAR” to “POSCAR_std”. One should use “POSCAR_std” to do the calculations within VASP, to be compatible with the program `irvsp` and TQC work [40–42, 44]. In the meantime, its standard output contains the WKS (q) for each atom and the irreps (ρ) for atomic orbitals (*i.e.*, s , p , d). These BRs ($\rho@q$) are the aBRs for the crystal. An example of `pos2aBR` output for Y_2C is shown in Fig. S1.

```
166 R-3m
\\
SN Mult. Wyck. Atom s p d Wyck. Name
 1  2  7 39  3  6  2  6c  Y
 2  1  9  6  2  2  0  3a  C
\\
SN Orb. @ Site Symm.
 1 Y-s @ 6c( 7) 3m(19) >>> (1) (2) (3) Basis
                               1 GM1 ;GM1 ; A1 ; z;x2+y2;z2
                               (1) (2) (3) Basis
                               1 GM1 ;GM1 ; A1 ; z;x2+y2;z2
                               3 GM3 ;GM3 ; E ; x,y;xz,yz;x2-y2,xy;Jx,Jy
 1 Y-p @ 6c( 7) 3m(19) >>> (1) (2) (3) Basis
                               1 GM1 ;GM1 ; A1 ; z;x2+y2;z2
                               3 GM3 ;GM3 ; E ; x,y;xz,yz;x2-y2,xy;Jx,Jy
                               3 GM3 ;GM3 ; E ; x,y;xz,yz;x2-y2,xy;Jx,Jy
 1 Y-d @ 6c( 7) 3m(19) >>> (1) (2) (3) Basis
                               1 GM1 ;GM1 ; A1 ; z;x2+y2;z2
                               3 GM3 ;GM3 ; E ; x,y;xz,yz;x2-y2,xy;Jx,Jy
                               3 GM3 ;GM3 ; E ; x,y;xz,yz;x2-y2,xy;Jx,Jy
 2 C-s @ 3a( 9) -3m(20) >>> (1) (2) (3) Basis
                               1 GM1+;GM1+; A1g; x2+y2;z2
 2 C-p @ 3a( 9) -3m(20) >>> (1) (2) (3) Basis
                               4 GM2-;GM2-; A2u; z
                               6 GM3-;GM3-; Eu ; x,y
```

FIG. S1. The standard output of `pos2aBR` for Y_2C . The notations of point group irreps under “(1)” are used in Bilbao Crystallographic Server [45–47]. The notations under “(2)” and “(3)” follow Ref. [48]

B. Irrep and BR analysis of Ca_2N and LaCl

Ca_2N and LaCl both crystallize in a hexagonal layered structure of SG $R\bar{3}m$ (SG #166) with only three atoms (two calcium and one nitrogen atoms) and four atoms (two lanthanum and two chlorine atoms) in the primitive rhombohedral unit cells, respectively. The basic building blocks of Ca_2N and LaCl are tightly bound triple-layer and quadruple-layer structures, respectively. For the triple-layer structure in Ca_2N , the nitrogen layer is sandwiched between two calcium layers in the sequence of Ca-N-Ca, while two hexagonal lanthanum layers are sandwiched between two hexagonal chlorine layers in the sequence of Cl-La-La-Cl for the quadruple-layer structures. The adjacent triple layers and quadruple layers are stacked loosely, resulting in the floating electrons moving into the interlayer gaps [Fig. S2(d)] and intralayer gaps [Fig. S2(e)], respectively. Atomic positions and aBRs of Ca_2N and LaCl are shown in Table S1 and Table S3, respectively.

The BS of Ca_2N shows three VBs dominated by N p orbitals in the energy range -4 eV to -1.5 eV, and a dispersive band traversing the Fermi level, as shown in Fig. S2(a). To understand the electrider essence in terms of TQC theory,

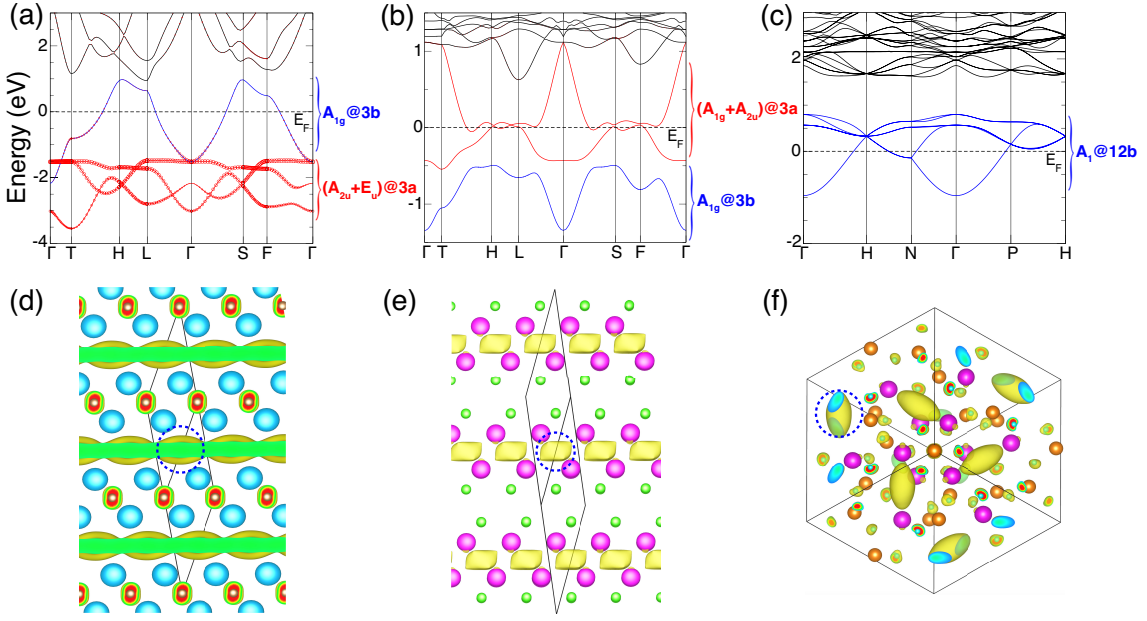


FIG. S2. (Color online) (a-c) The BSs of Ca_2N , LaCl , and C12A7 , respectively. The spectral weight of N p orbitals for Ca_2N is denoted by the size of the red circles. (d-f) The calculated PED of the blue-colored bands for Ca_2N , LaCl , and C12A7 , respectively.

we calculate the irreps and BRs for the four bands near the Fermi level, as shown in Table S2. It is clear that the BR $A_{1g}@3b$ from these bands is an eBR, and generated by electrons located at the vacancy $3b$, suggesting that Ca_2N is an electride.

The BS of LaCl is shown in Fig. S2(b), and irreps and BRs for the three bands near the Fermi level of LaCl are shown in Table S4. Since there are band inversions at Γ and T, the irreps for the highest band at Γ and T are unknown. After carefully analyzing the BRs, one can get that the unknown irreps should be $\text{GM1}+(1)$ and $\text{T2}-(1)$. At last, we find that these bands support an eBR $A_{1g}@3b$ generated by electrons located at the vacancy $3b$, which suggests that LaCl is an electride.

TABLE S1. Atomic positions and aBRs of Ca_2N (SG $R\bar{3}m$).

Atom	WKS(q)	Site symm.	Conf.	Irreps(ρ)	aBRs($\rho@q$)
Ca	6c	3m	$3p^64s^2$	$s : A_1$	$A_1@6c$
				$p_z : A_1$	$A_1@6c$
				$p_x, p_y : E$	$E@6c$
N	3a	$-3m$	$2s^22p^3$	$s : A_{1g}$	$A_{1g}@3a$
				$p_z : A_{2u}$	$A_{2u}@3a$
				$p_x, p_y : E_u$	$E_u@3a$

TABLE S2. Irreps and BRs for the four bands near the Fermi level of Ca_2N .

	Γ	T	F	L
Bands	$\text{GM1}+(1)$	$\text{T2}-(1)$	$\text{F2}-(1)$	$\text{L2}-(1)$
	$\text{GM2}-(1)$	$\text{T2}-(1)$	$\text{F2}-(1)$	$\text{L2}-(1)$
	$\text{GM3}-(2)$	$\text{T3}-(2)$	$\text{F1}-(1)$	$\text{L1}-(1)$
			$\text{F1}+(1)$	$\text{L2}-(1)$
BRs				
$A_{2u}@3a$	$\text{GM2}-(1)$	$\text{T2}-(1)$	$\text{F2}-(1)$	$\text{L2}-(1)$
$E_u@3a$	$\text{GM3}-(2)$	$\text{T3}-(2)$	$\text{F1}-(1) \oplus \text{F2}-(1)$	$\text{L1}-(1) \oplus \text{L2}-(1)$
$A_{1g}@3b$	$\text{GM1}+(1)$	$\text{T2}-(1)$	$\text{F1}+(1)$	$\text{L2}-(1)$

TABLE S3. Atomic positions and aBRs of LaCl (SG $R\bar{3}m$).

Atom	WKS(q)	Site symm.	Conf.	Irreps(ρ)	aBRs($\rho@q$)
La	6c	3m	$5s^25p^66s^25d^1$	s : A_1	$A_1@6c$
				p_z : A_1	$A_1@6c$
				p_x, p_y : E	$E@6c$
				d_{z^2} : A_1	$A_1@6c$
Cl	6c	3m	$3s^23p^5$	$d_{xy}, d_{xz}, d_{yz}, d_{x^2-y^2}$: E	$E@6c$
				s : A_1	$A_1@6c$
				p_z : A_1	$A_1@6c$
				p_x, p_y : E	$E@6c$

TABLE S4. Irreps and BRs for the three bands near the Fermi level of LaCl. The question mark (“?”) stands for any one-dimensional (1D) irrep (*i.e.*, the unknown irrep) at Γ and T. After analyzing the BRs, one then can conjecture that the unknown irrep should be GM1+(1) and T2-(1).

	Γ	T	F	L
Bands	GM1+(1)	T2-(1)	F1+(1)	L2-(1)
	GM2-(1)	T1+(1)	F1+(1)	L1+(1)
	? (1)	? (1)	F2-(1)	L2-(1)
BRs (one of cases)				
$A_{1g}@3a$	GM1+(1)	T1+(1)	F1+(1)	L1+(1)
$A_{2u}@3a$	GM2-(1)	T2-(1)	F2-(1)	L2-(1)
$A_{1g}@3b$	GM1+(1)	T2-(1)	F1+(1)	L2-(1)

C. Irrep and BR analysis of C12A7

C12A7 with low work function (about 0.6 eV) is a room-temperature electride, whose unusual properties are due to its special crystalline structure with the SG of $I\bar{4}3d$ (SG #220). The stoichiometric cubic unit cell is represented by the formula $[\text{Ca}_{24}\text{Al}_{28}\text{O}_{64}]^{4+} \cdot [\text{O}^{2-}]_2$. The first term $[\text{Ca}_{24}\text{Al}_{28}\text{O}_{64}]^{4+}$ denotes a positively charged framework built of twelve cages, while the second term $[\text{O}^{2-}]_2$ represents two extra-framework oxygen ions occupying two of the twelve cages. By reduction treatment, the extra-framework oxygen ions can be replaced with electrons acting as anions, leading to the formation of the electride C12A7. Atomic positions and aBRs of C12A7 are shown in Table S5.

The BS of C12A7 is shown in Fig. S2(c), irreps and BRs for the six bands near the Fermi level of C12A7 are shown in Table S6. This six bands support an eBR $A_1@12b$ located at the vacancy $12b$, as shown in Fig. S2(f), which confirms that C12A7 is an electride.

TABLE S5. Atomic positions and aBRs of C12A7 (SG $I\bar{4}3d$).

Atom	WKS(q)	Site symm.	Conf.	Irreps(ρ)	aBRs($\rho@q$)
Ca	24d	2	$3p^64s^2$	s : A	$A@24d$
				p_z : A	$A@24d$
				p_x, p_y : B	$B@24d$
Al(1)	12a	-4	$3s^23p^1$	s : A	$A@12a$
				p_z : B	$B@12a$
				p_x : 2E	${}^2E@12a$
				p_y : 1E	${}^1E@12a$
Al(2)	16c	3	$3s^23p^1$	s : A_1	$A_1@16c$
				p_z : A_1	$A_1@16c$
				p_y : 2E	${}^2E@16c$
				p_x : 1E	${}^1E@16c$
O(1)	16c	3	$2s^22p^4$	s : A_1	$A_1@16c$
				p_z : A_1	$A_1@16c$
				p_y : 2E	${}^2E@16c$
				p_x : 1E	${}^1E@16c$
O(2)	48e	1	$2s^22p^4$	s : A	$A@48e$
				p_z, p_x, p_y : A	$A@48e$

TABLE S6. Irreps and BRs for the six bands near the Fermi level of C12A7.

	Γ	H	P	N
Bands	GM1(1)	H4H5(6)	P3(4)	N1(2)
	GM5(3)		P2(2)	N1(2)
	GM3(2)			N1(2)
BRs				
$A_1@12b$	$GM1(1)\oplus GM5(3)\oplus GM3(2)$	$H4H5(6)$	$P3(4)\oplus P2(2)$	$3N1(2)$

D. The evolution of mBJ BSs of A_2B

A_2B ($A = \text{Ca, Sr, and Ba}$; $B = \text{As, Sb, and Bi}$) is a large family of isostructural materials hosting similar electronic structures. They are known as electriles before, and recently draw intensive research interest due to the presence of nontrivial band topology. In order to better understand the relation between these two different properties, we calculate the mBJ BSs of A_2B , as shown in Fig. S3. Although increasing the weights of the pnictogen elements doesn't change the BS too much, the heavier alkaline earth metal in A_2B leads to the larger band inversion.

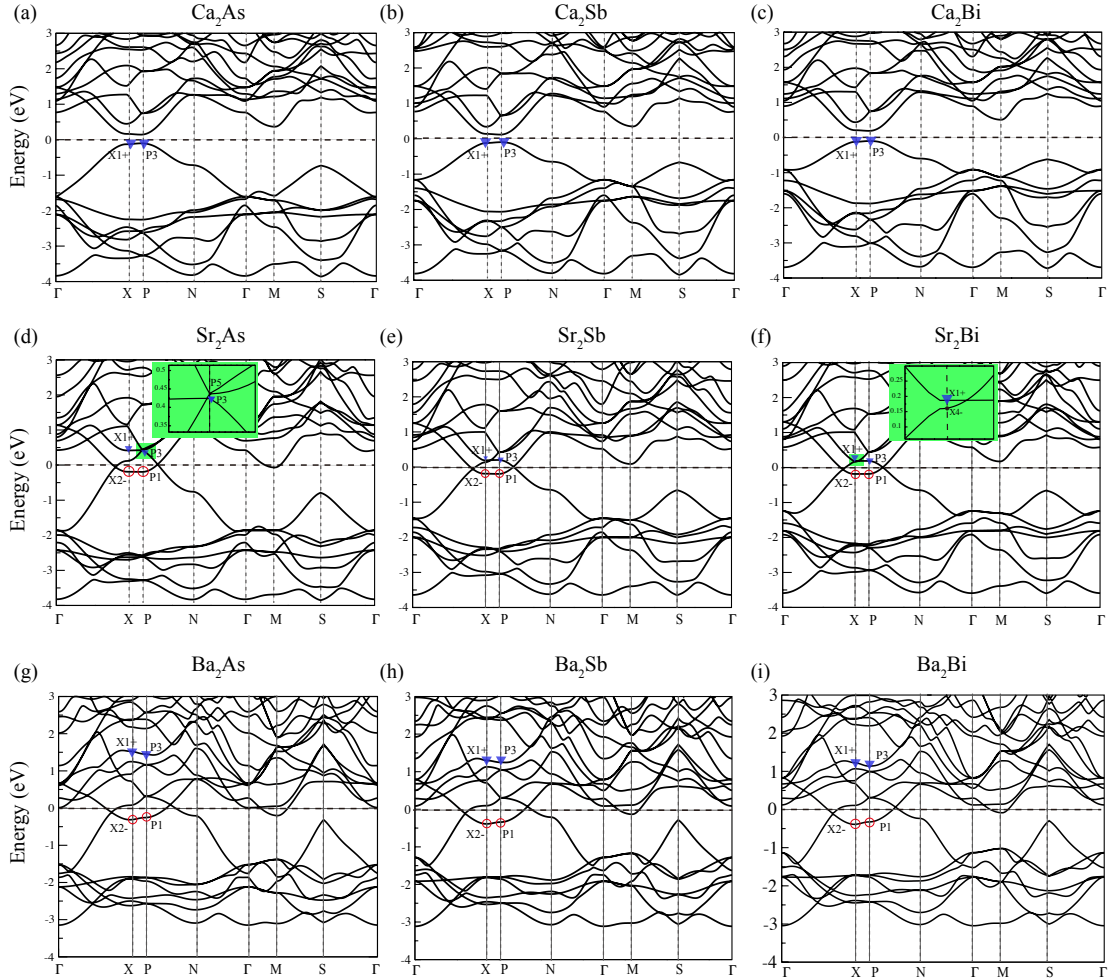


FIG. S3. (Color online) The calculated BSs of A_2B family. For the trivial BSs without band inversion, the bands marked by the blue-filled triangles are occupied by charges at vacancies, and the bands marked by red-hollow circles unoccupied. It shows that the band inversion increases as the weights of the pnictogen elements increase.

E. The absorption of hydrogen atoms in Ba_3CrN_3

Table S7 shows the aBRs of Ca_5P_3 , which are used to understand the absorption of hydrogen atoms in this material. Similar to Ca_5P_3 , we perform the BR analysis on Ba_3CrN_3 with the SG of $P6_3/m$ (SG #176), which was previously predicted to be a 1D topological electride with anomalous Dirac plasmon [49]. Fig. S4(a) shows the BS of Ba_3CrN_3 , where the obtained irreps are marked out. Based on the aBRs of Ba_3CrN_3 shown in Table S8, the BR analysis shows that the blue-solid bands belong to the eBR of $A_{1g}@2b$, induced by excess electrons at the vacancies $2b$. By absorbing hydrogen atoms at the vacancies, these bands are removed from E_F for $\text{Ba}_3\text{CrN}_3\text{H}$ [Fig. S4(b)]. The insulating BS is consistent with recent measurements, since the charge-balanced compound $\text{Ba}_3\text{CrN}_3\text{H}$ has been obtained in experiments [50]. So the results of hydrogen absorption clearly show that electrides exhibit excess electrons at cavities.

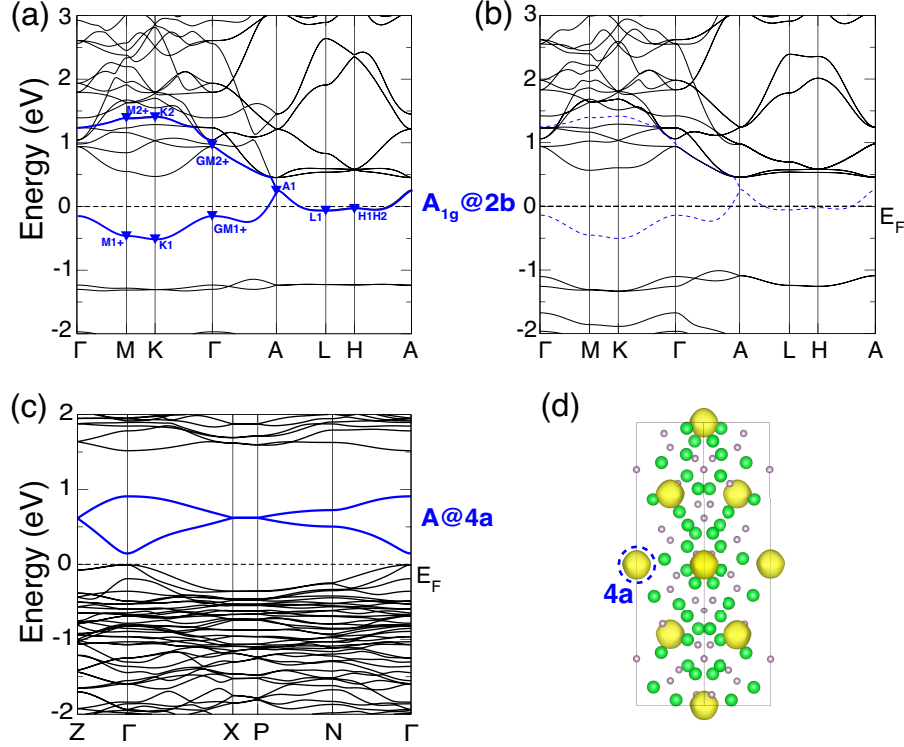


FIG. S4. (Color online) The BSs of Ba_3CrN_3 (a), $\text{Ba}_3\text{CrN}_3\text{H}$ (b) and Sr_3P_2 (c). The floating bands (blue-solid) denote electronic states of excess electrons, whose eBRs can be well determined by the obtained irreps. To facilitate the comparison, the irreps of particular bands are marked out, and the “disappeared” floating bands are depicted by blue-dashed lines in (b) for $\text{Ba}_3\text{CrN}_3\text{H}$. (d) The PED of Sr_3P_2 .

TABLE S7. Atomic positions and aBRs of Ca_5P_3 (SG $P6_3/mcm$).

Atom	WKS(q)	Site symm.	Conf.	Irreps(ρ)	aBRs($\rho@q$)
Ca(1)	4d	32	$3p^64s^2$	$s : A_1$	$A_1@4d$
				$p_z : A_2$	$A_2@4d$
				$p_x, p_y : E$	$E@4d$
Ca(2)	6g	$mm2$	$3p^64s^2$	$s : A_1$	$A_1@6g$
				$p_z : A_1$	$A_1@6g$
				$p_y : B_2$	$B_2@6g$
				$p_x : B_1$	$B_1@6g$
P	6g	$mm2$	$3s^23p^3$	$s : A_1$	$A_1@6g$
				$p_z : A_1$	$A_1@6g$
				$p_y : B_2$	$B_2@6g$
				$p_x : B_1$	$B_1@6g$

TABLE S8. Atomic positions and aBRs of Ba₃CrN₃ (SG $P6_3/m$).

Atom	WKS(q)	Site symm.	Conf.	Irreps(ρ)	aBRs($\rho@q$)
Ba	6h	m	$5s^26s^25p^6$	s : A'	$A'@6h$
				p_x, p_y : A'	$A'@6h$
				p_z : A''	$A''@6h$
Cr	2c	$\bar{6}$	$3d^54s^1$	s : A'	$A'@2c$
				p_z : A''	$A''@2c$
				p_x : ${}^2E'$	${}^2E'@2c$
				p_y : ${}^1E'$	${}^1E'@2c$
				d_{z^2} : A'	$A'@2c$
				$d_{x^2-y^2}$: ${}^2E'$	${}^2E'@2c$
				d_{xz} : ${}^2E''$	${}^2E''@2c$
				d_{xy} : ${}^1E'$	${}^1E'@2c$
N	6h	m	$2s^22p^3$	s : A'	$A'@6h$
				p_x, p_y : A'	$A'@6h$
				p_z : A''	$A''@6h$
				d_{xz} : ${}^1E''$	${}^1E''@2c$
				d_{yz} : ${}^1E''$	${}^1E''@2c$

F. The BR analysis of the predicted electrides

In order to further understand the eBRs contributed from the states at vacancies, we tabulate the atomic positions and aBRs for NaBaO, K₂O, Sr₆GaN₅ and Sr₃P₂ in Tables S9, S10, S11 and S12, respectively. We here focus on another predicted electride, *i.e.*, Sr₃P₂. The GGA BS of Sr₃P₂ with the SG of I42d (SG #122) is presented in Fig. S4(c). The BR analysis indicates that two blue-colored bands (above E_F) form the eBR of $A@4b$. The PED of the two bands is plotted in Fig. S4(d), agreeing well with the BR analysis.

Since the CBs of both Sr₃P₂ and Sr₆GaN₅ are well separated from other bands, and the charge centers of these CBs are well defined at the cavities, we propose that Sr₃P₂ and Sr₆GaN₅ are potential electrides; namely, they could be electrides after electron doping. As shown in Figs. 5(a,c) in the main text, the floating bands of K₂O and Sr₆GaN₅ are the highest CBs. To occupy these bands, electron doping with suitable elements is employed. For K₂O and Sr₆GaN₅, 50% oxygen and 50% gallium are doped with F and Ge, respectively. The electronic structures of K₂O_{0.5}F_{0.5} and Sr₆Ga_{0.5}Ge_{0.5}N₅ are studied with the virtual crystal approximation method, and the results are shown in Fig. S5. It is clearly that the floating bands are half filled, and the overall BSs almost don't change except an overall BS shift.

TABLE S9. Atomic positions and aBRs of NaBaO (SG $P4/nmm$).

Atom	WKS(q)	Site symm.	Conf.	Irreps(ρ)	aBRs($\rho@q$)
Ba	2c	4mm	$5s^26s^25p^6$	s : A_1	$A_1@2c$
				p_z : A_1	$A_1@2c$
				p_x, p_y : E	$E@2c$
O	2c	4mm	$2s^22p^4$	s : A_1	$A_1@2c$
				p_z : A_1	$A_1@2c$
				p_x, p_y : E	$E@2c$
Na	2c	4mm	$3s^1$	s : A_1	$A_1@2c$

TABLE S10. Atomic positions and aBRs of K₂O (SG $Fm\bar{3}m$).

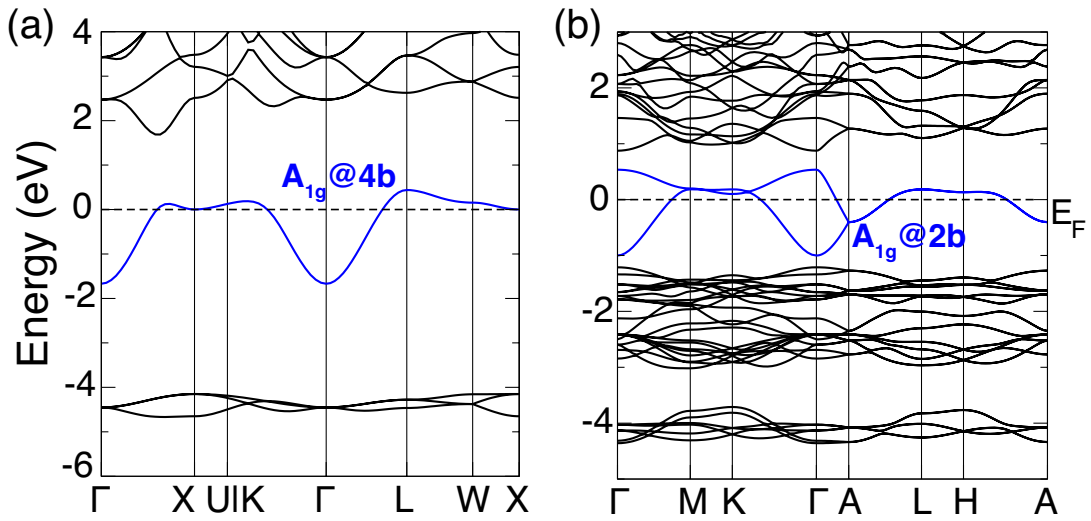
Atom	WKS(q)	Site symm.	Conf.	Irreps(ρ)	aBRs($\rho@q$)
O	4a	$m\bar{3}m$	$3p^64s^2$	s : A_{1g}	$A_{1g}@4a$
				p_x, p_y, p_z : T_{1u}	$T_{1u}@4a$
K	8c	$\bar{4}3m$	$3p^64s^2$	s : A_1	$A_1@8c$
				p_x, p_y, p_z : T_1	$T_1@8c$

TABLE S11. Atomic positions and aBRs of Sr_6GaN_5 (SG $P6_3/mcm$).

Atom	WKS(q)	Site symm.	Conf.	Irreps(ρ)	aBRs($\rho@q$)
Sr	$12k$	m	$5s^26s^25p^6$	s : A'	$A'@12k$
				p_x, p_y : A'	$A'@12k$
				p_z : A''	$A''@12k$
Ga	$2a$	$\bar{6}2m$	$4s^24p$	s : A'_1	$A'_1@2a$
				p_z : A''_2	$A''_2@2a$
				p_y : E'	$E'@2a$
				d_{z^2} : A'_1	$A'_1@2a$
				$d_{x^2-y^2}, d_{xy}$: E'	$E'@2a$
				d_{xz}, d_{yz} : E''	$E''@2a$
N(1)	$4d$	32	$2s^22p^3$	s : A_1	$A_1@4d$
				p_z : A_2	$A_2@4d$
				p_x, p_y : E	$E@4d$
N(2)	$6g$	$mm2$	$2s^22p^3$	s : A_1	$A_1@6g$
				p_z : A_1	$A_1@6g$
				p_y : B_2	$B_2@6g$
				p_x : B_1	$B_1@6g$

TABLE S12. Atomic positions and aBRs of Sr_3P_2 (SG $I\bar{4}2d$).

Atom	WKS(q)	Site symm.	Conf.	Irreps(ρ)	aBRs($\rho@q$)
Sr(1)	$16e$	1	$5s^26s^25p^6$	$s; p_x; p_y; p_z$: A	$A@16e$
Sr(2)	$16e$	1	$5s^26s^25p^6$	$s; p_x; p_y; p_z$: A	$A@16e$
Sr(3)	$16e$	1	$5s^26s^25p^6$	$s; p_x; p_y; p_z$: A	$A@16e$
P(1)	$8c$	2	$3s^23p^3$	$s; p_z$: A	$A@8c$
				$p_x; p_y$: B	$B@8c$
P(2)	$8d$	2	$3s^23p^3$	$s; p_z$: A	$A@8d$
				$p_x; p_y$: B	$B@8d$
P(3)	$16e$	1	$3s^23p^3$	$s; p_x; p_y; p_z$: A	$A@16e$

FIG. S5. (Color online) (a,b) The BSs of $\text{K}_2\text{O}_{0.5}\text{F}_{0.5}$ and $\text{Sr}_6\text{Ga}_{0.5}\text{Ge}_{0.5}\text{N}_5$, respectively.